

Plasma Jets Production at Laser-Burnt-Through Foils and their Interaction with Secondary Targets

O. Renner¹, J. Cihelka¹, L. Juha¹, J. Krása¹, E. Krouský¹, J. Nejd¹, J. Skála¹, A. Velyhan¹,
T. Pisarczyk², T. Chodukowski², Z. Kalinowska², A. Kasperczuk², P. Pisarczyk³,
R. Liska⁴, M. Šmíd⁴, P. Váchal⁴, J. Velechovský⁴, J. Ullschmied⁵

¹Institute of Physics, v.v.i., Academy of Sciences Czech Rep., Na Slovance 2, 182 21 Prague, Czech Republic

²Institute of Plasma Physics and Laser Microfusion, 00908 Warsaw, Poland

³Warsaw University of Technology, ICS, 00665 Warsaw, Poland

⁴Czech Technical University in Prague, FNSPE, Břehová 7, 115 19 Prague, Czech Republic

⁵Institute of Plasma Physics, v.v.i., Academy of Sciences Czech Rep., Prague, Czech Republic
renner@fzu.cz

Abstract. Interest in laser-driven plasma jets is justified by their relevance for high-energy-density laboratory astrophysics and for the fusion directed research. In experiments carried out on the iodine laser system PALS, interactions of plasma jets with solid surfaces are studied in context with phenomena accompanying the material erosion and migration at plasma facing components, i.e., an issue of paramount importance for development of future fusion devices. The energetic ions were produced at burnt-through foils with low-to-high atomic numbers (Al, Ag, Ta). The formation of the outflow plasma was investigated using the three-frame interferometry, the observed density distribution was complemented by numerical modeling of the plasma parameters based on the Arbitrary Lagrangian Eulerian code PALE. The found optimum conditions for the jet production were used in a design of alternate experimental configurations. The interaction of the directional plasma flows with secondary targets was studied via x-ray imaging, optical and high-resolution x-ray spectroscopy. The examples of jet applications for investigating the transition phenomena at surfaces of plasma-exposed solids are presented.

1. Introduction

An interest in laser-driven plasma jets is connected with their relevance for two substantially different scientific disciplines. In high-energy-density laboratory astrophysics, the jets launching, propagation and interaction with surrounding media are studied to verify diverse theoretical models and to interpret large-scale astrophysical situations [1-5]. In the fusion directed research, the energetic particle jets are investigated like prospective ignitors in alternate schemes of the inertial confinement fusion [6-8]. Further very important fusion-relevant applications are connected with studies of the material erosion and migration at plasma facing components, particularly in context with a search for optimum inner-wall materials of fusion devices [9]. The acquisition of detailed experimental data on transient phenomena accompanying the interaction of energetic plasma jets with surfaces of solid materials (hereafter plasma-wall interaction, PWI) contributes to the understanding of the material response to heavy loads of charged particles and provides information needed for a development of advanced simulation techniques assisting in a design of fusion reactors [10].

Various mechanisms of the energy transfer in the near-wall region (e.g., ion deceleration and stopping [11], shock wave generation [12], formation of highly excited Rydberg states [13] or hollow atoms with multiple inner vacancies [14], charge transfer processes [15] and ion neutralization [13]) are to be studied at well-defined environmental conditions with the smallest possible perturbations introduced, e.g., by 2D effects in strongly non-homogeneous media with variable macroscopic parameters. A large span of laser-matter interaction regimes

available at nano-, pico- and femtosecond lasers provides a unique opportunity to produce plasma jets with the desired particle composition, energy and degree of collimation appropriate for PWI studies. A survey of the previous research in this field can be found in papers [16-18]. In contrast to hitherto experiments claiming difficult formation of laser-produced plasma jets at targets with lower atomic number $Z \leq 13$ [3, 19, 20], we report a successful production of well-collimated jets at burnt-through Al foils. The conditions for the jet production were optimized using the three-frame interferometry, results of interferometric observations are complemented by a numerical modeling based on the Arbitrary Lagrangian Eulerian code PALE. Finally we provide examples of the jet applications in the PWI research.

2. Interferometric optimization of plasma jets

The experiment was performed using the iodine laser system at the PALS Research Centre in Prague [21]. The laser beam delivering 40-200 J of frequency-tripled radiation (438 nm) in a pulse length of 0.3-0.35 ns (full width at half maximum) was incident onto the primary, jet-producing target (0.8- μm -thick Al, 1- μm -thick Ag or 0.5- μm -thick Ta foils) either perpendicularly to its surface or inclined by an angle of $\alpha = 30^\circ$ from the target normal. In both experimental configurations schematically shown in Fig. 1, the foils burn through well before the laser pulse maximum [11], and the expanding plasma plume created at the rear (non-irradiated) foil surface propagates primarily along the direction of the target normal. The alternate target-beam configurations determine the regime of the plasma interaction with the secondary target. At normal incidence (Fig. 1a), the plasma jet strikes the secondary target pre-ionized by the action of the transmitted laser light, i.e., the PWI effects are complemented by the near-wall interaction of two counter-propagating plasmas. In the oblique incidence case (Fig. 1b), the laser beam does not hit the secondary target and the expanding plasma interacts with the unperturbed surface (though potentially pre-heated by fast particles emitted from the primary plasma and by its radiation), thus creating a better-characterized environment for PWI studies. Further we demonstrate that by optimizing the laser interaction with the primary target, well collimated low-Z jets can be produced in both configurations.

The standard diagnostic complex used in the PALS PWI experiments (time-resolved x-ray imaging of plasma expansion, optical spectroscopy and several x-ray spectrometers [18]) was complemented by a three-frame laser interferometric system with independent folding-wave-type interferometers [22]. The temporally and spatially resolved electron density n_e of the expanding plasma was determined by applying the Abel transformation on the measured 2D phase distribution of the plasma probing radiation. The diagnostic beams were split-off from the main iodine laser beam and frequency-doubled, thus limiting the maximum measurable electron density to $2.6 \times 10^{21} \text{ cm}^{-3}$. The delay between contiguous frames was set to 3 ns.

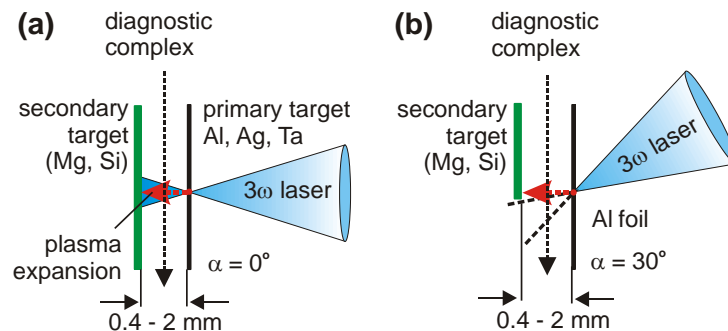


Fig. 1. Alternate schemes of plasma jets production at burnt-through foils and their interaction with secondary targets.

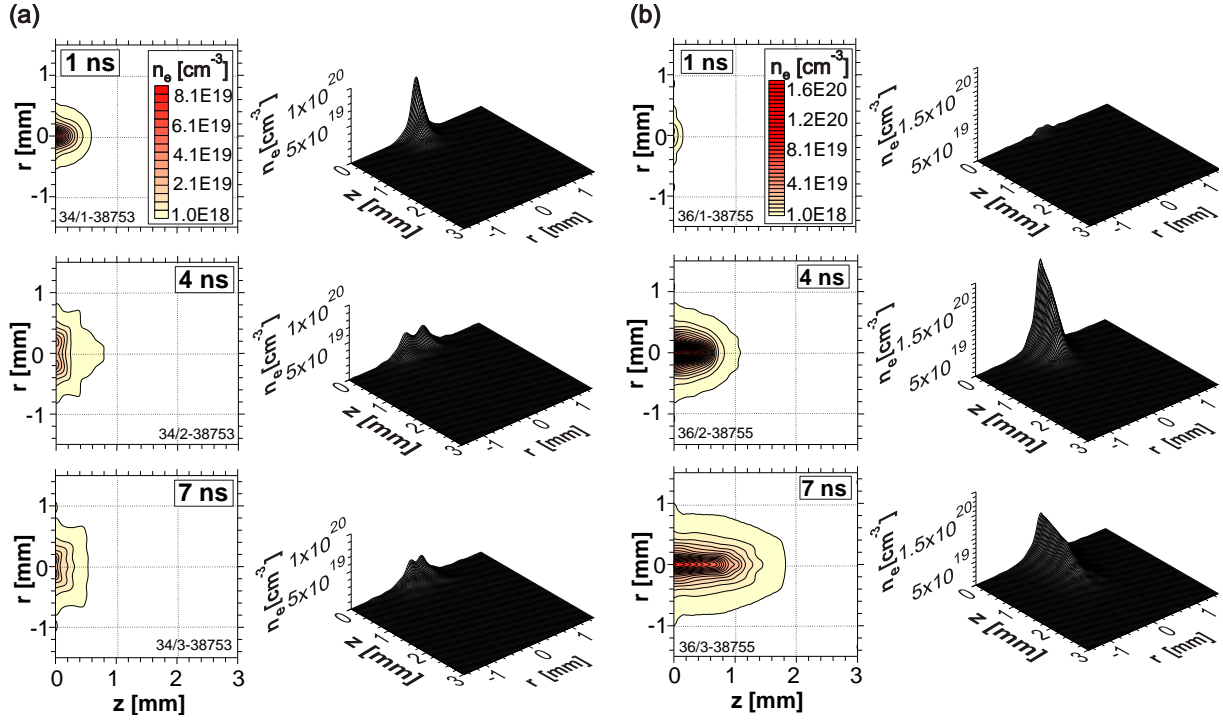


Fig. 2. Interferometric sequences characterizing distribution of the plasma electron density at a rear side of the Al foil irradiated by the laser beam focused to a radius $R=40\ \mu\text{m}$ (a) and $R=300\ \mu\text{m}$ (b).

The recorded interferograms were used to optimize the conditions for the plasma jet generation in the transmission geometry. The sample interferometric sequences presented in Fig. 2 visualize the electron density distribution by equidensity lines. The outer plasma contour refers to the $n_e = 10^{18}\ \text{cm}^{-3}$, the step between adjacent lines is $5 \times 10^{18}\ \text{cm}^{-3}$. The shown sequences illustrate the plasma creation at two extreme conditions of the Al foil irradiation. Both n_e distributions were recorded at normal incidence with the same laser energy (64 J). The frame timing relates to the laser pulse maximum, the distance r is measured along the foil surface and z along its normal. Figure 2a corresponds to the minimum focal spot radius $R = 40\ \mu\text{m}$. This case is not favorable for the jets forming. The semispherical plasma flow is spatially restricted and exhibits collateral jets resulting in a strong electron density depression on the axis (cf. flat equidensity lines well visible at 4 and 7 ns). In contrast, the beam defocused to $R = 300\ \mu\text{m}$ (Fig. 2b) created an expanding plasma with much larger spatial extent and considerably higher density on the jet axis. Despite a relatively broad low-density plume surrounding the dense plasma core, the Al jet is well developed, transversal density gradients are sufficiently steep and the maximum observed densities exceed $1.5 \times 10^{20}\ \text{cm}^{-3}$. These results can be explained by pinching effects of the axial plasma expansion affected by the annular target irradiation (which is more pronounced when defocusing the laser beam). The increased focal spot radius results in an annular target irradiation which is the main mechanism responsible for the plasma jet formation [23]. When keeping the laser energy in the range of 40-70 J, the optimal conditions for the plasma jet formation at 0.8- μm -thick Al foil occurred at the focal spot radius $R = 300\ \mu\text{m}$ (independently of positioning the minimum focal point in front and behind the foil surface). For higher-Z foils (Ag and Ta), the optimum corresponded to slightly smaller laser beam foci, $R = 150\ \mu\text{m}$.

Similar characteristics of the jet formation were found when irradiating the Al foils at oblique incidence ($\alpha = 30^\circ$). In that case, the plasma jets are characterized by a slightly larger length (above 2 mm) and by a deformed front in the initial expansion phase (Fig. 3, $t = 1$ and 4 ns).

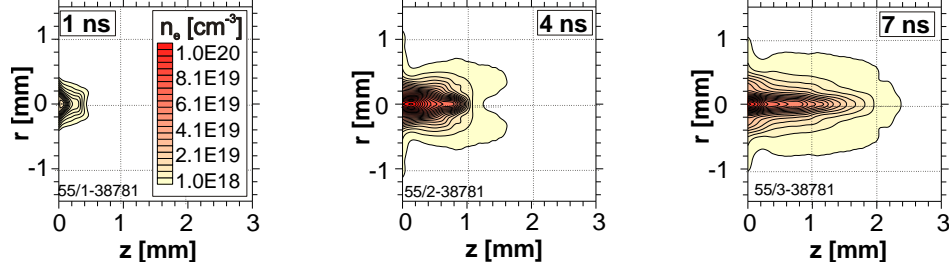


Fig. 3. Electron density distribution in the expanding plasma jet observed at oblique incidence of the laser beam (42 J, $R = 300 \mu\text{m}$) onto the 0.8- μm -thick Al foil.

Such shape of the plasma front refers to the elliptical focal spot created on the foil at oblique laser incidence. The focal spot dimensions in the horizontal plane (corresponding to the major axis of the ellipse) and in the vertical plane (minor axis) differ, hence the directional characteristics of the plasma expansion in both planes are different. Early stage interaction between spherical and axial components of both plasmas leads to a creation of external wings accompanying the axial ion outflow in the plasma front. The density characterizing these lateral wings is rather low, thus they do not essentially influence the formation of dense plasma jets. In the later stages of the plasma expansion, the electron density distribution on the front becomes typical for the plasma jet structure formation (cf. Fig. 3, $t = 7 \text{ ns}$).

The electron density distributions observed at both normal and oblique laser incidence onto the Al foil show that the axial velocities of the plasma jets are approximately the same (about $2.5 \times 10^7 \text{ cm/s}$). The directional characteristics of the generated plasma jets comply with requirements for the successful investigation of the PWI processes [11]. To demonstrate this, in Fig. 4 we present a typical n_e distribution recorded when irradiating the double-foil Ta/Mg target at the laser oblique incidence (42 J, $R = 150 \mu\text{m}$, foil spacing 1 mm). The Ta plasma (in particular, its dense core) propagates between both foils in a laminar flow and no large-scale plasma turbulences are visible. The dynamics of the Ta ions trapping at the secondary target is characterized by a z -dependence of the linear electron density and by the time-dependent electron content in the inter-target space. The n_e distributions shown in Fig. 4 demonstrate the influence of the secondary target on the axial plasma outflow. Contrary to the free plasma expansion (where linear density monotonically decreases with the distance from the target),

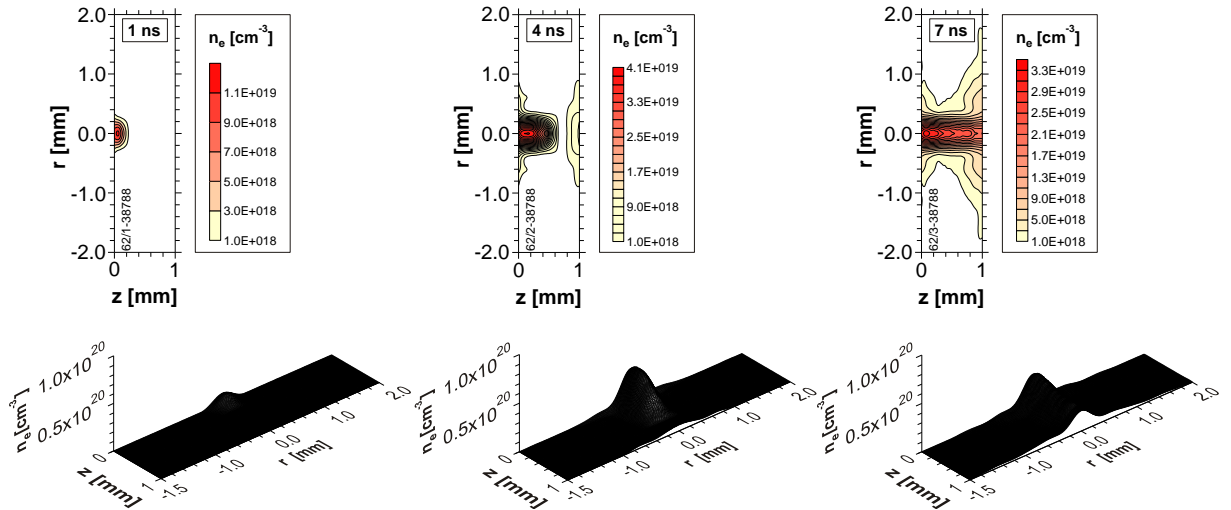


Fig. 4. Interaction of the plasma jet generated at oblique laser incidence on the 0.5- μm -thick Ta foil with the secondary Mg target.

the presence of the secondary target results in the practical stopping of the axial plasma flow. At $t = 4$ ns already, the Ta jet forms a counter-propagating plasma at the secondary Mg target. Ongoing weaker plasma outflow further increases the electron density near the secondary target (Fig. 4, $t=7$ ns) where the Ta plasma laterally dissipates. This effect however introduces only small perturbations into the observation of the energetic plasma jet interaction with the secondary target. Consequently, optimized jets represent a well-defined model environment for investigating transient phenomena at surfaces of plasma-exposed solids.

3. Theoretical simulations of plasma expansion

A qualitative explanation of the jets formation follows from 2D simulations of the plasma evolution performed using the Prague Arbitrary Lagrangian Eulerian hydrocode (PALE) [24, 25]. The code models the laser-target-plasma interaction by using a set of Euler equations, i.e., the hydrodynamic conservation laws for mass, momentum and energy of compressible fluid, with additional terms in the energy equation to capture laser absorption and heat transfer. The system is closed by an equation of state (EOS) coupling density, pressure, internal energy and temperature. In the simulations presented below we used either EOS for perfect polytropic gas (with the reduced maximum ionization degree) or Quotidian EOS [26].

ALE strategy combines features of the Eulerian and Lagrangian treatment of computational meshes. It can be described by three repeating blocks: (i) the Lagrangian stage, which advances the solution in time using a purely Lagrangian scheme, moving the mesh along with the fluid, (ii) the rezoning stage, where the distorted computational mesh is improved to prevent a loss or failure of the computational accuracy and (iii) the remapping stage, where the solution is conservatively remapped from the Lagrangian mesh to the rezoned one. The position and velocity are assigned to mesh nodes, while the thermodynamic variables (density, pressure and temperature) are defined in cells. The concepts of the subcell pressure forces and the artificial viscosity are used to prevent the mesh from bad deformations by the shock waves and to dissipate the kinetic energy into the internal one. All computations have been performed in the cylindrical geometry. The simple Winslow formula was chosen for rezoning, however spurious mesh changes were prevented already in the Lagrangian part by restricting the nodes motion in cold regions of the mesh. Remapping of the solution between the meshes was performed by the piecewise linear interpolation of the mass, momentum and energy with the Barth-Jespersen limiting, swept region integration and a posteriori repair [27].

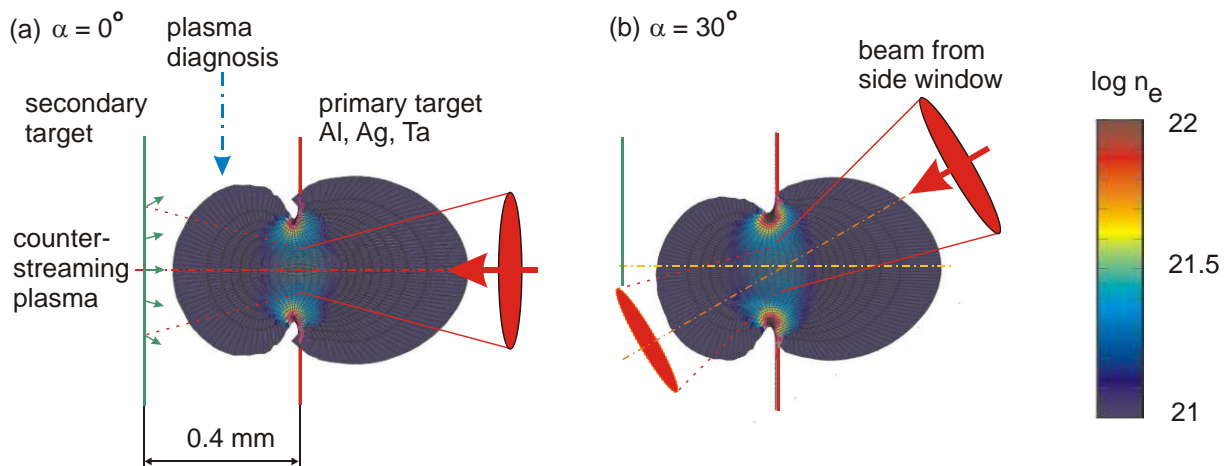


Fig. 5. PALE simulations of the Al plasma expansion at normal (a) and oblique laser incidence (b).

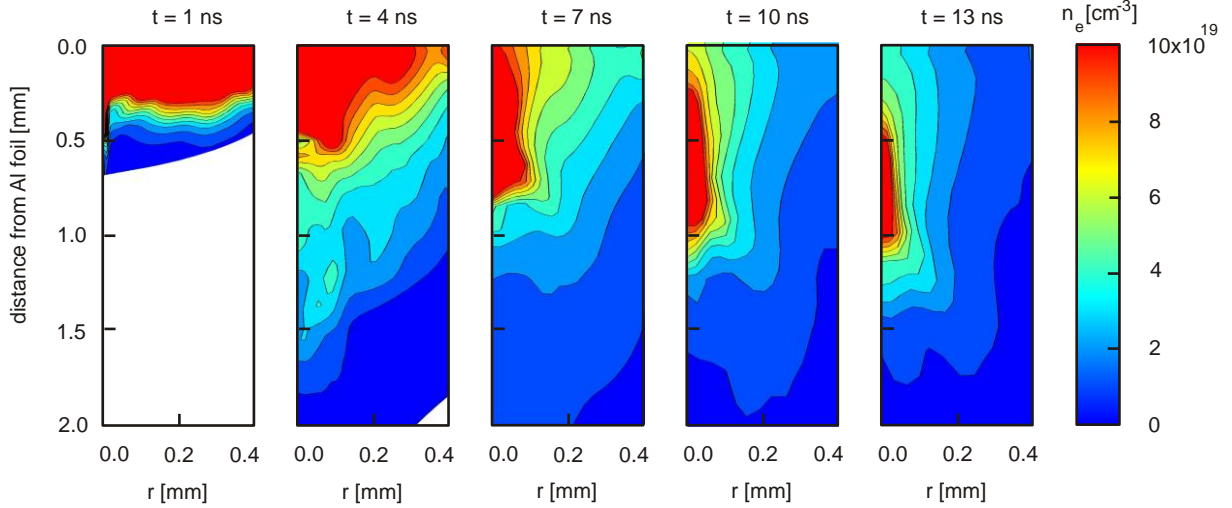


Fig. 6. Modeling of the jet formation at Al foil irradiated by the laser beam with a central depression.

The heat conductivity was approximated by the classical Spitzer-Harm formula. Unrealistically high numerical heat fluxes were decreased by the heat flux limiting. The laser propagated till the critical surface where the given part of its energy was absorbed.

The PALE simulations of the plasma evolution at double-foil targets have recently been published in papers [11, 18, 25], here we concentrate to the interaction of the laser beams with single foils. The first example presented in Fig. 5 shows the electron density distribution at the laser-exploded Al foils corresponding to the laser pulse maximum. In both cases, i.e., the normal (a) and the oblique laser incidence (b), the foil was irradiated by the tightly focused laser beam (42 J, $R=40\ \mu\text{m}$). Under these conditions, the foil burns through well before the laser maximum and the plasma expansion from the front (irradiated) and rear surface of the foil is approximately semispherical. At the normal laser incidence, the radiation transmitted through the hole burnt in the foil is strong enough to produce the relatively dense counter-propagating plasma at the prospective secondary target. At the oblique incidence, the plasma plume created at the rear side of the foil again propagates roughly perpendicularly to the foil surface, thus demonstrating the possibility to investigate the genuine plasma-wall interaction non-affected by the pre-plasma created by the transmitted laser beam.

The temporal evolution of the plasma shown in time-dependent frames at Fig. 6 (the time scale relates to the laser maximum) explains one of the alternate mechanisms for the jets creation. The simulations were performed for the $0.8\text{-}\mu\text{m}$ -thick Al foil irradiated at the normal incidence by the laser beam (3ω , 0.3 ns, 42 J) defocused to $R=300\ \mu\text{m}$. The calculations using the EOS for an ideal gas assumed the realistic laser beam profile with the central depression corresponding to the actual intensity distribution in the defocused PALS beam. Under these conditions, the modeling predicts the creation of plasma jets without requiring the presence of complementary mechanisms, e.g., radiative cooling of the plasma. The detailed quantitative explanation of the jets creation and propagation should however include all key mechanisms (radiation, magnetic fields, interaction with the surrounding media) which may contribute to the jets formation [4].

4. Selected spectroscopic applications

In this section, we briefly provide several examples of jet applications. Selected phenomena accompanying the PWI are studied by advanced optical and x-ray spectroscopic methods.

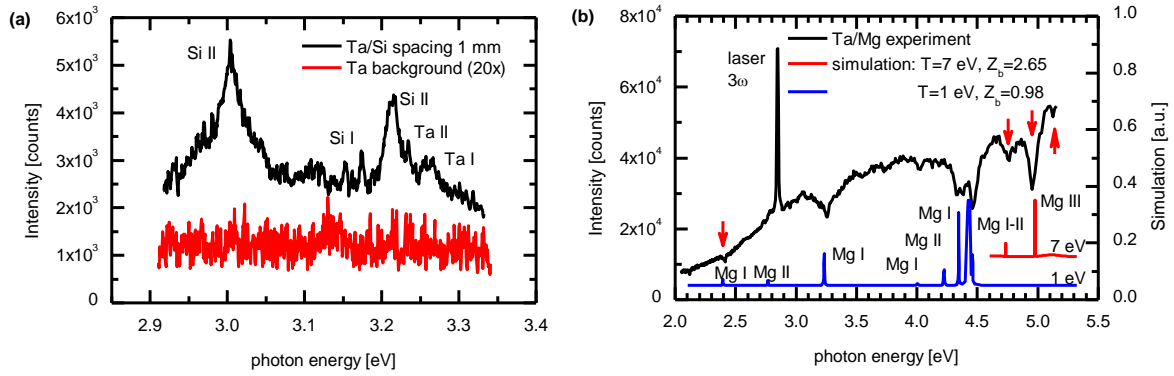


Fig. 7. Characterization of the plasma-wall interaction via optical spectroscopy.

The optical spectra were recorded using the Oriel Instruments imaging spectrometer MS260i. The line of sight of the micro-lens connected to the optical fiber cable was approximately perpendicular to the plasma jet propagation. The lens covered the plasma emission area with the diameter of approximately 1.5 mm, the spectral resolution of the used grating amounted to 1.5×10^{-3} eV. The images were taken in single laser shots using the CCD detection system. The spectra shown in Fig. 7a characterize the trapping of the Ta ions at the secondary massive Si target. The plasma jet was produced at the 0.5- μ m-thick Ta foil irradiated by the laser beam (60 J, $R = 150 \mu\text{m}$) at the oblique incidence, the inter-target distance was set to 1 mm. The plasma self-emission was recorded 1 μs after the laser pulse maximum with the exposure time of 1 ms. The Ta spectrum taken without the presence of the secondary target was rather weak, the Ta background shown in Fig. 7a is multiplied by a factor of 20. The insertion of the secondary target revealed in an enhanced emission close to the Si surface. The well resolved transitions Ta I and II indicate the ion trapping and recombination in the near-wall interaction area, the strongest spectral transitions Si I and II prove the excitation and single ionization of the Si target by the plasma impact.

The spectrum shown in Fig. 7b was recorded at the double-foil Ta (0.5 μm)/Mg (2 μm) system with the inter-target spacing of 1 mm. The laser beam (69 J, $R = 150 \mu\text{m}$) was incident perpendicularly to the Ta surface, the spectrum was taken 30 ns after the laser pulse maximum with the acquisition time of 200 μs . The interaction of the Ta jet with the counter-propagating Mg plasma is visualized via the absorption structure in the Ta quasi-continuum, the main pumped transitions in the singly and doubly ionized Mg are identified. The simulations performed using the PrismSPECT code [28] estimated the main parameters of the two-components recombining plasma to the ion density $1 \times 10^{17} \text{ cm}^{-3}$, temperature 7 eV and 1 eV, and the average charge 2.65 and 0.98, respectively. The detailed evaluation of all these spectra is in progress, the future application of the optical diagnostics to the investigation of the plasma recombination processes is envisaged.

Selected examples of the x-ray spectroscopic investigation of the PWI phenomena via the laser-produced plasma jets are presented in Fig. 8. The first application concerns the precise measurements of the ion deceleration close to the walls. The Al ions produced at the laser oblique incidence were incident onto the secondary Mg target positioned at a distance of 550 μm , the plasma interaction with the wall was investigated via the x-ray self-emission of the H-like Al ions. The spatially resolved spectra were observed at an angle of 0.8° to the Al foil surface by using the vertical-dispersion Johann spectrometer (VJS) [29]. The reconstructed mirror-symmetric spectra of the Al Ly α group are shown in Fig. 8a.

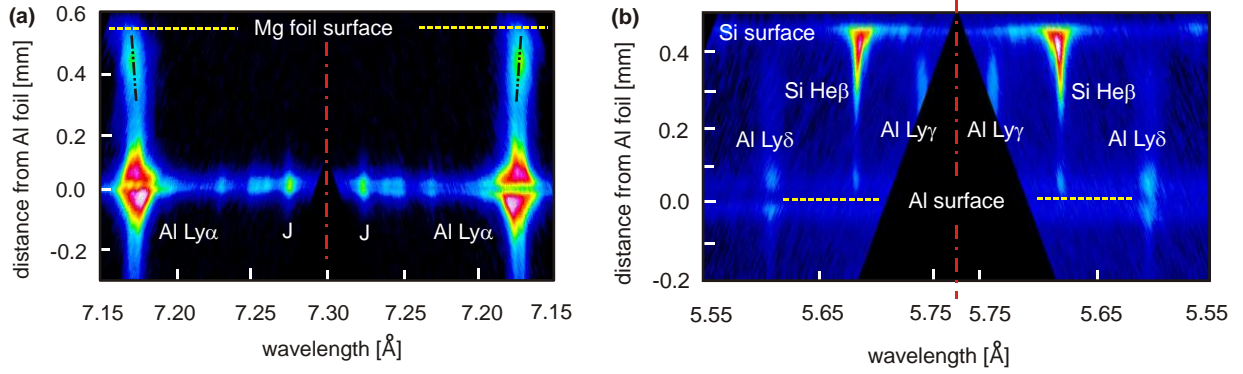


Fig. 8. The blue shift of the spectral line Al Ly α corresponds to a gradual deceleration of the Al ions near the Mg foil surface (a). Spatially resolved spectral record of the strongly collisional plasma produced at Al/Si (PMMA-coated) target at normal laser incidence (b).

The spectra analysis relates a distinct blue Doppler shift (dot-dot-dash line) of the Al Ly α resonance line close to the Mg foil surface to the gradual Al ion deceleration from the velocity $\sim 5 \times 10^7$ cm/s to their full stopping at the Mg surface. The spectroscopically determined maximum ion velocity exceeds that derived from the interferometry. This discrepancy is justified by different periods of data collection: the interferometric data acquisition spans within 1-7 ns, whereas the strong Ly α emission occurs at 0.6-1.3 ns after the laser pulse maximum [30].

The second VJS spectral record presented in Fig. 8b corresponds to a more complicated interaction scenario. The plasma jet was produced on the Al foil irradiated at normal laser incidence, the secondary target (massive Si coated by the 0.5- μ m-thick layer of PMMA, C₅H₈O₂) was positioned at a distance of 450 μ m. After burning through the Al foil, the laser produced the counter-propagating plasma on the secondary target. Due to the strong plasma collisionality, the Al jet visualized via the Al Ly γ emission does not penetrate to the surface of the secondary target (but the Si He β emission is distinctly seen in the Al foil position which indicates the longer-duration plasma production in massive Si). The analysis of the spatially resolved Al Ly γ emission observed at distances 100 – 140 μ m from the secondary target revealed local depressions in the red wing of the line profiles which were tentatively ascribed to the charge exchange phenomena between the Al and fully stripped C ions. The detailed interpretation of these spectroscopic signatures is currently in progress.

5. Conclusions

The production of energetic plasma jets at laser-burnt-through foils was studied with respect to their applications in the fusion directed research. By varying the parameters of the laser-matter interaction, the production of high-aspect-ratio plasma jets at burnt-through foils was optimized. Selected applications of the jets interactions with the secondary targets demonstrate their usefulness in PWI investigation.

This research was supported by the Czech Science Foundation Grant No. P205/10/0814, and CR Ministry of Education, Youth and Sports, grants No LC528 and MSM6840770022.

References

- [1] RYUTOV, D.D., et al., "Criteria for scaled laboratory simulations of astrophysical MHD phenomena", *Astrophys. J. Suppl. Series* **127** (2000) 465.
- [2] REMINGTON, B.A., et al., "Experimental astrophysics with high power lasers and Z pinches", *Rev. Mod. Phys* **78** (2006) 755.
- [3] GREGORY, C.D., et al., "Astrophysical jet experiments with colliding laser-produced plasmas", *Astrophys. J.* **676**, (2008) 420.
- [4] BOUQUET, S., et al., "From lasers to the universe: Scaling laws in laboratory astrophysics", *High Energy Density Physics* **6**, 368-380 (2010).
- [5] NICOLAÏ, Ph., et al., "Experimental evidence of multimaterial jet formation with lasers", *Phys. Plasmas* **17** (2010) 112903.
- [6] DITTRICH, T.R., et al., "Review of indirect-drive ignition design options for the National Ignition Facility", *Phys. Plasmas* **6**, (1999) 2164.
- [7] KEY, M.H., "Status of and prospects for the fast ignition inertial fusion concept", *Phys. Plasmas* **14** (2007) 055502.
- [8] HONRUBIA, J.J., et al., "Fast ignition of inertial fusion targets by laser-driven carbon beams ", *Phys. Plasmas* **16** (2009) 102701.
- [9] ROTH, J., et al., "Plasma-wall interaction: a complex combination of surface processes critical for thermo-nuclear fusion", *Journal of Physics: Conference Series* **100** (2008) 062003.
- [10] INSEPOV, Z., et al., "Surface erosion and modification by ions studied by computer simulation", *Nucl. Instr. Meth. Phys. Res B* **258** (2007) 172.
- [11] RENNER, O., et al., "Laser-produced plasma-wall interaction", *Laser Part. Beams* **27**, (2009) 725.
- [12] ZEL'DOVICH, Ya.B., RAIZER, Yu.P., *Physics of shock waves and high-temperature hydrodynamic phenomena*, Dover Publications, Mineola, N.Y. (2002).
- [13] BURGDÖRFER, J., et al., "Above-surface neutralization of highly charged ions: The classical over-the-barrier model", *Phys. Rev. A* **44**, (1991) 5674.
- [14] WINTER, H., AUMAYR, F., "Hollow atoms", *J. Phys. B: At. Mol. Opt. Phys.* **32**, (1999) R39.
- [15] DALIMIER, E., et al., "Experimental determination of rate coefficients of charge exchange from x-dips in laser-produced plasmas", *J. Phys. B: At. Mol. Opt. Phys.* **40** (2007) 909.
- [16] MAZING, M.A., et al., "Interaction of a laser-produced plasma with a solid surface", *Phys. Rev; A* **32**, (1985) 3695.
- [17] SHEVELKO, A.P., et al., "Structure and intensity of x-ray radiation in a laser plasma-wall interaction", *Proc. SPIE* **4505**, (2001) 171.
- [18] RENNER, O., et al., "Direct spectroscopic observation of ion deceleration accompanying laser plasma-wall interaction", *Journal of Physics: Conference Series* **244**, (2010) 022024.
- [19] KASPERCZUK, A., et al., "Stable dense plasma jets produced at laser power densities around 10^{14} W/cm²", *Phys. Plasmas* **13**, (2006) 062704.
- [20] KURAMITSU, Y., et al., "Jet formation in counterstreaming plasmas produced by high-power laser beams", *Journal of Physics: Conference Series* **244** (2010) 042009.
- [21] JUNGWIRTH, K., et al., "The Prague Asterix Laser System PALS", *Phys. Plasmas* **8** (2001)2495.
- [22] KASPERCZUK, A., PISARCZYK, T., "Application of automated interferometric system for investigation of the behavior of a laser-produced plasma in strong external magnetic fields", *Optica Applicata* **31** (2001) 571.

- [23] KASPERCZUK, A., et al., "Influence of target material on structure of the plasma outflow produced by a partly defocused laser beam", *Applied Physics Letters* **94** (2009) 081501.
- [24] KUCHARIK, M., et al., "Laser plasma simulations by Arbitrary Lagrangian Eulerian method", *J. Phys. IV France* **133** (2006) 167.
- [25] LISKA, R., et al., "ALE method for simulations of laser-produced plasmas", in *Finite Volumes for Complex Applications VI* (FOŘT, J., FÜRST, J., HALAMA, J., HERBIN, R., HUBERT, F. Eds.), Springer, 2011 (in press).
- [26] MORE, R.M., et al., "A new quotidian equation of state (QEOS) for hot dense matter", *Phys. Fluids* **31**(1988) 3059.
- [27] KUCHARIK, M., et al., "An efficient linearity-and-bound-preserving remapping method", *J. Comput. Phys.* **188** (2003) 462.
- [28] MACFARLANE, J.J., et al., "SPECT3D – A multi-dimensional CR code for generating diagnostic signatures based on hydrodynamics and PIC simulation output", *High Energy Density Phys.* **3** (2007) 181.
- [29] RENNER, O., et al., "High-luminosity, high-resolution x-ray spectroscopy of the laser-produced plasma by vertical-geometry Johann spectrometer", *Rev. Sci. Instr.* **68** (1997) 2393.
- [30] RENNER, O., et al., "Plasma-wall interaction studies with optimized laser-produced jets", (in preparation).